Supporting Information

Dipole Moment Regulation of Small Molecule Quinone Mediator Boosts Long-Term Cycling Stability for Decoupled Water Electrolysis

AJing Song, Xin Jin, Yuan Wei, Chunmao Xiong, Tongna Shi, Yuanyuan Ma, Jianping Yang**

State Key Laboratory for Advanced Fiber Materials, College of Materials Science and Engineering, Institute of Functional Materials, Donghua University Shanghai 201620, China.

*Corresponding authors: yyma@dhu.edu.cn; jianpingyang@dhu.edu.cn

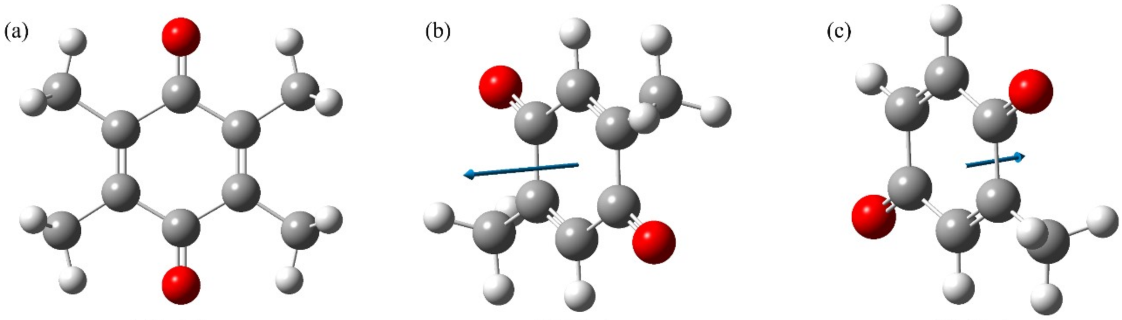

0.00 Debye **0.00 Debye** **0.84 Debye**

Fig. S1 Dipole moments of (a) TMBQ, (b) DMBQ, and (c) MBQ. The arrow indicates the direction of the dipole moment.

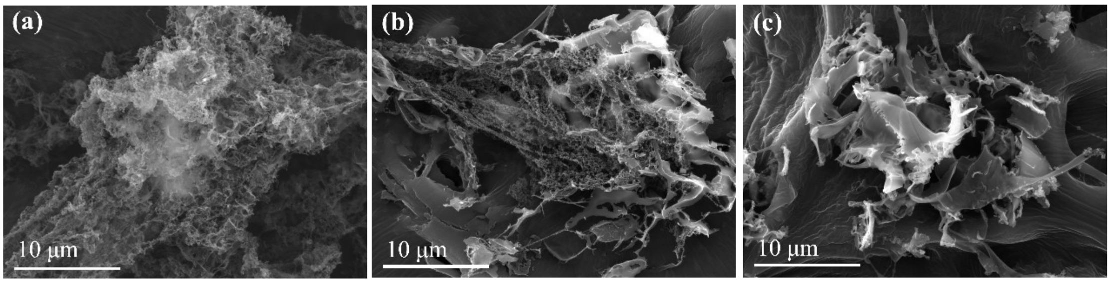

Fig. S2 The SEM images of (a) TMBQ, (b) DMBQ, and (c) MBQ.

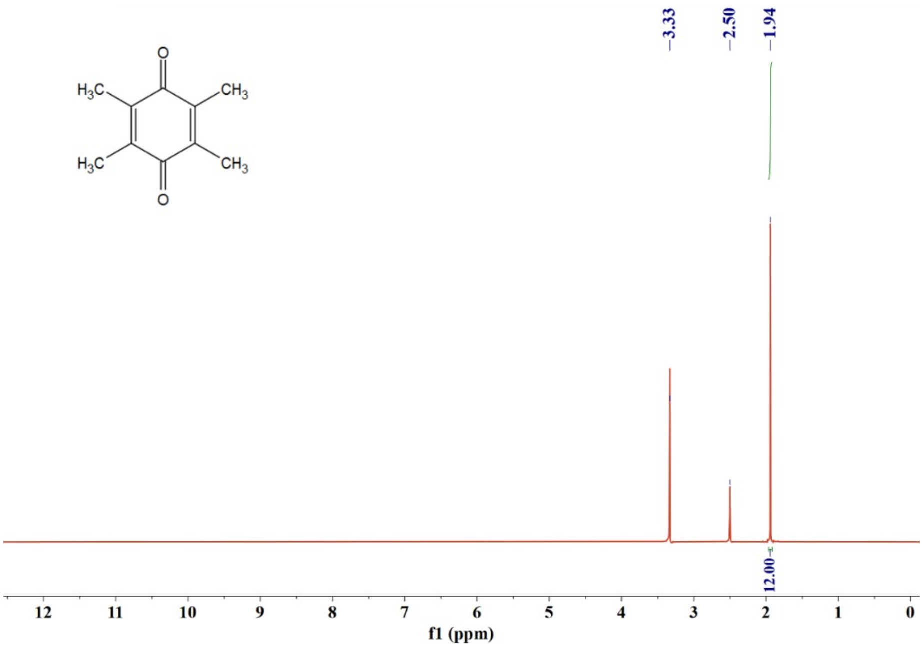

Fig. S3 ^{1}H NMR spectrum of TMBQ.

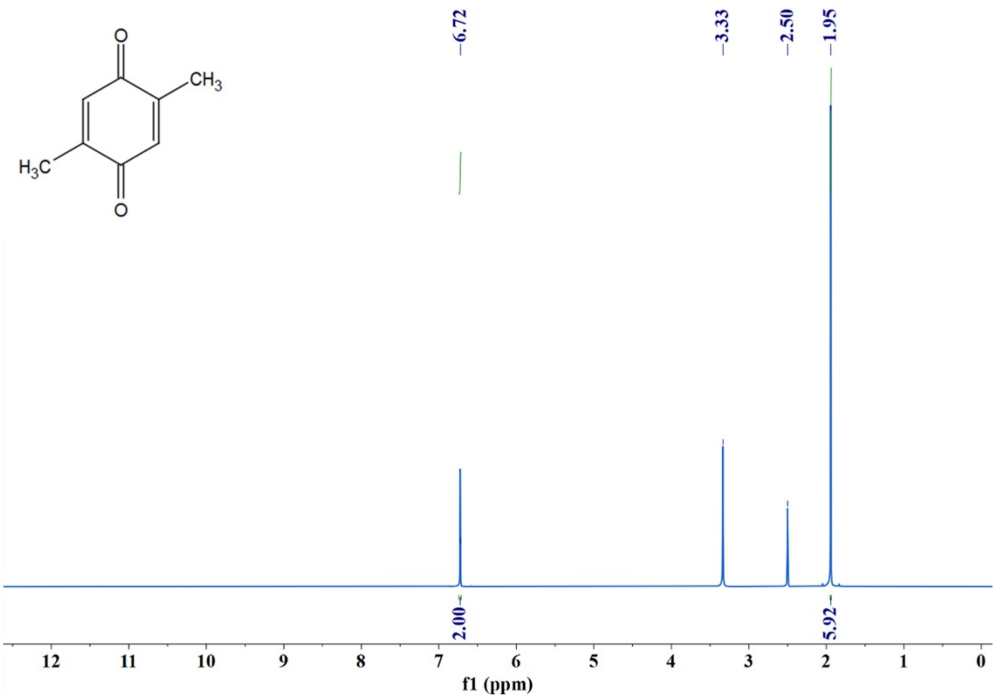

Fig. S4 ^{1}H NMR spectrum of DMBQ.

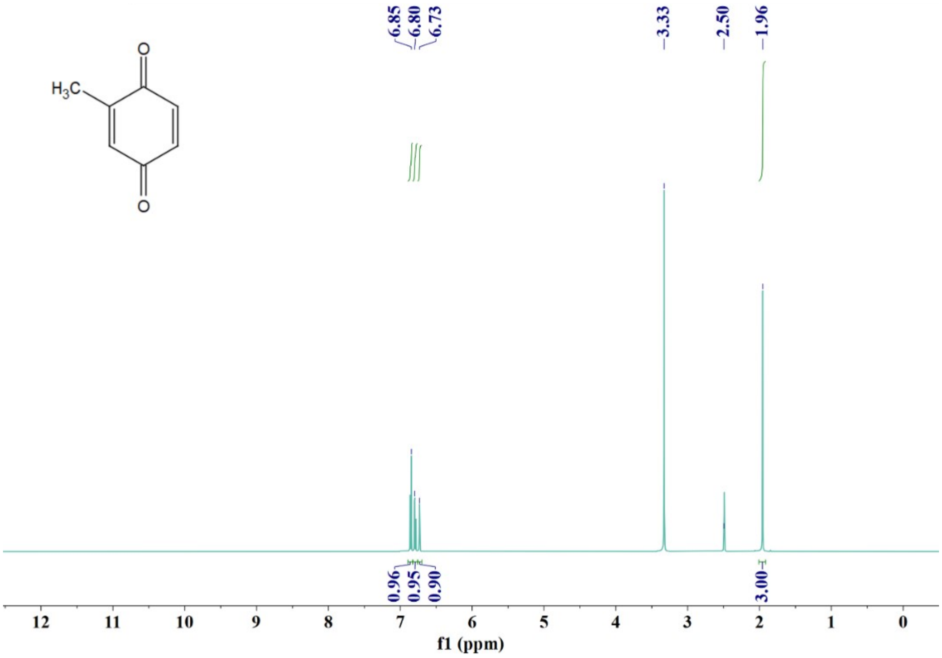

Fig. S5 ^{1}H NMR spectrum of MBQ.

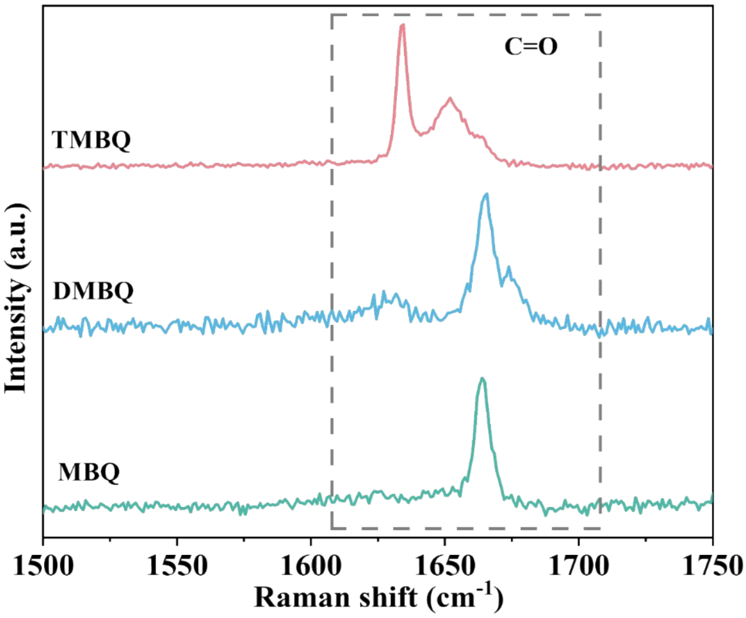

Fig. S6 The Raman spectra of powdered TMBQ, DMBQ, and MBQ.

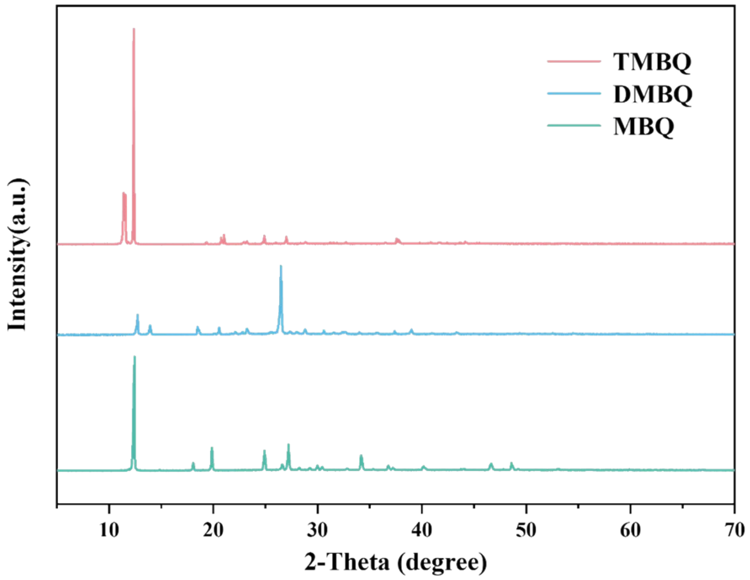

Fig. S7 The XRD patterns of TMBQ, DMBQ, and MBQ.

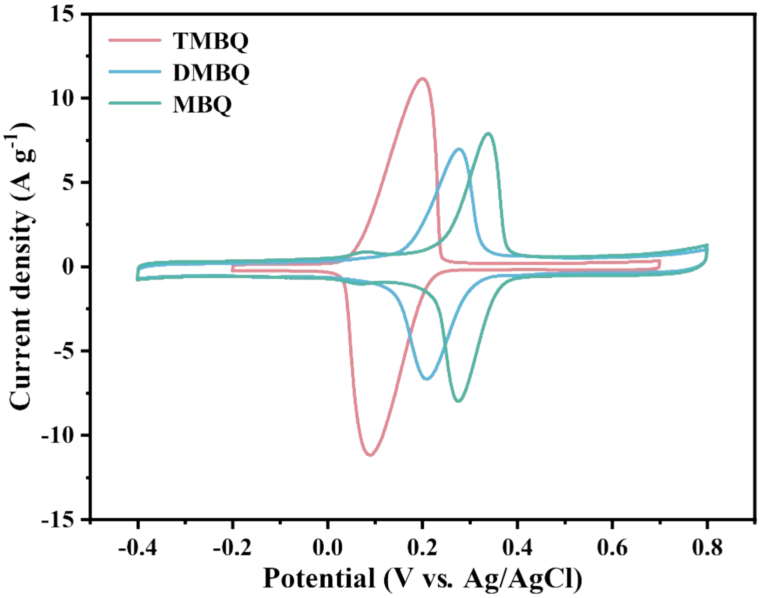

Fig. S8 CV curves at the scan rate of 4 mV s^{-1} of TMBQ, DMBQ, and MBQ.

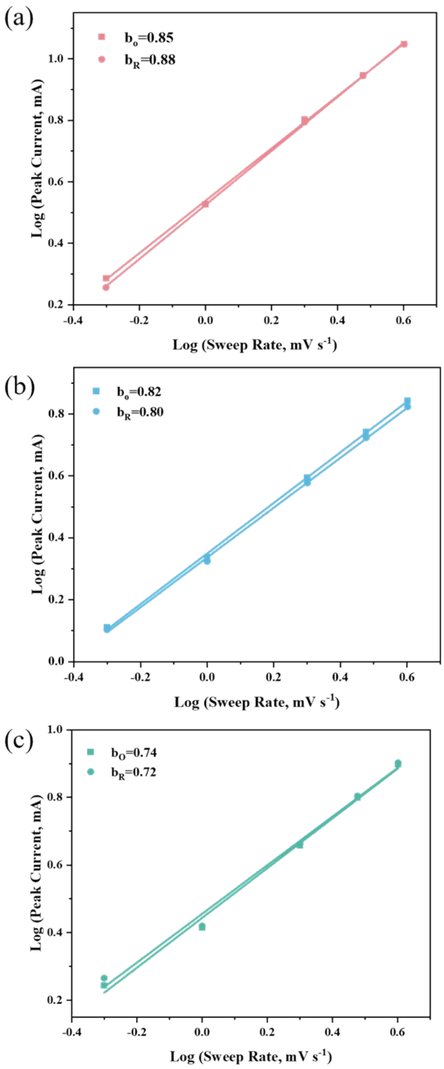

Fig. S9 Plots of lg(v) against lg(i_p) correspond to the CV curves of (a) TMBQ, (b) DMBQ, and (c) MBQ.

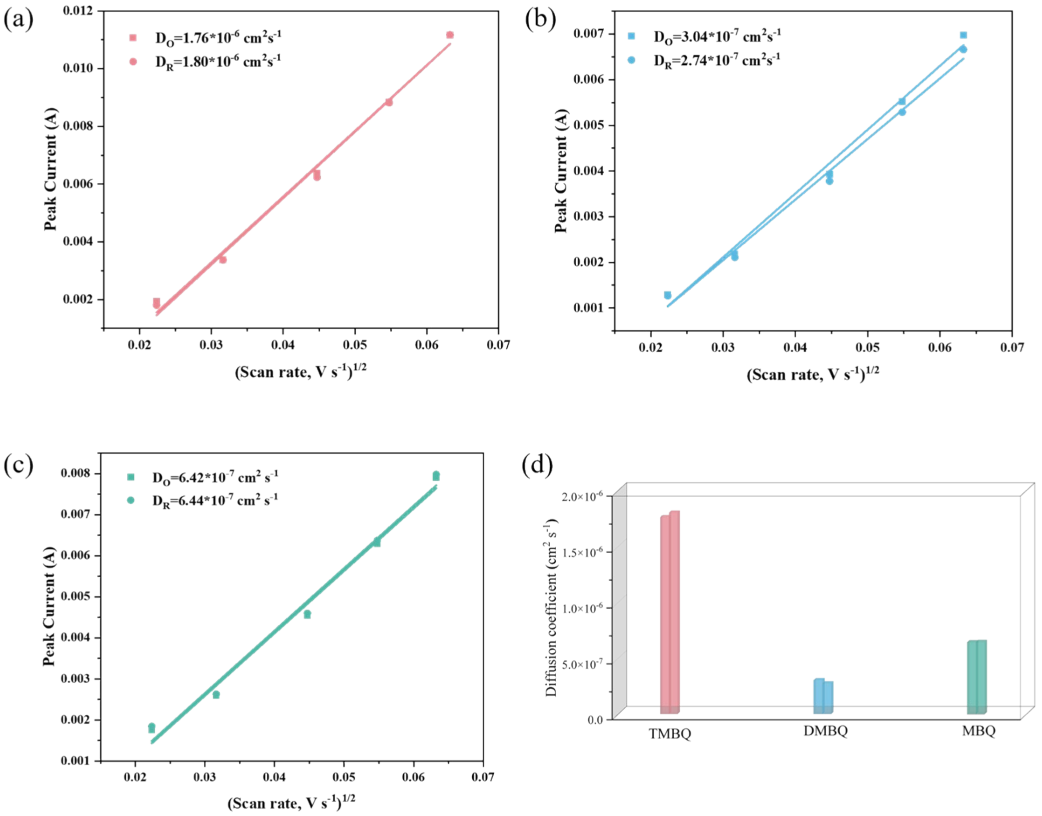

Fig. S10 The corresponding plots of peak current vs. (scan rate)$^{1/2}$ according to the CV curves of (a) TMBQ, (b) DMBQ, (c) MBQ, and (d) summary comparison of three in 0.5 M H_2SO_4.

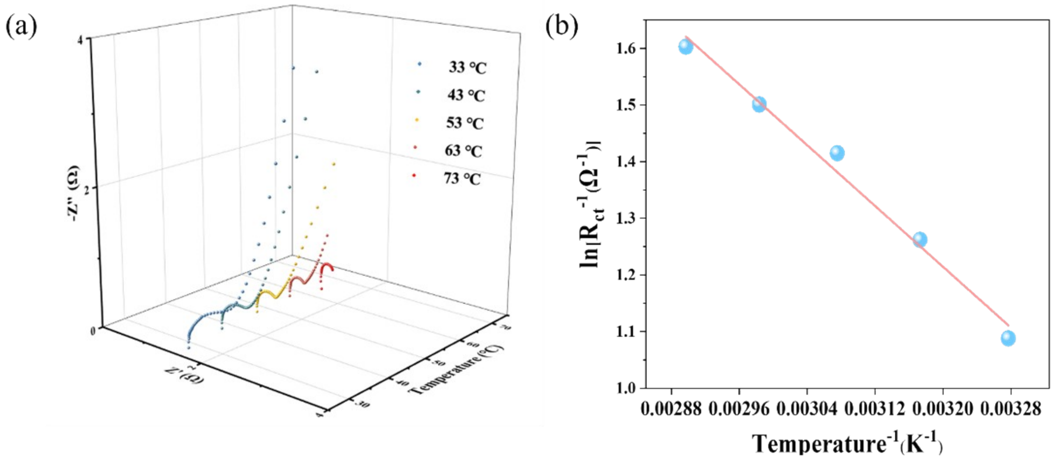

Fig. S11 (a) Nyquist plots were obtained from electrochemical impedance spectroscopy measurements. (b) Charge-transfer resistance of TMBQ electrode as a function of temperature.

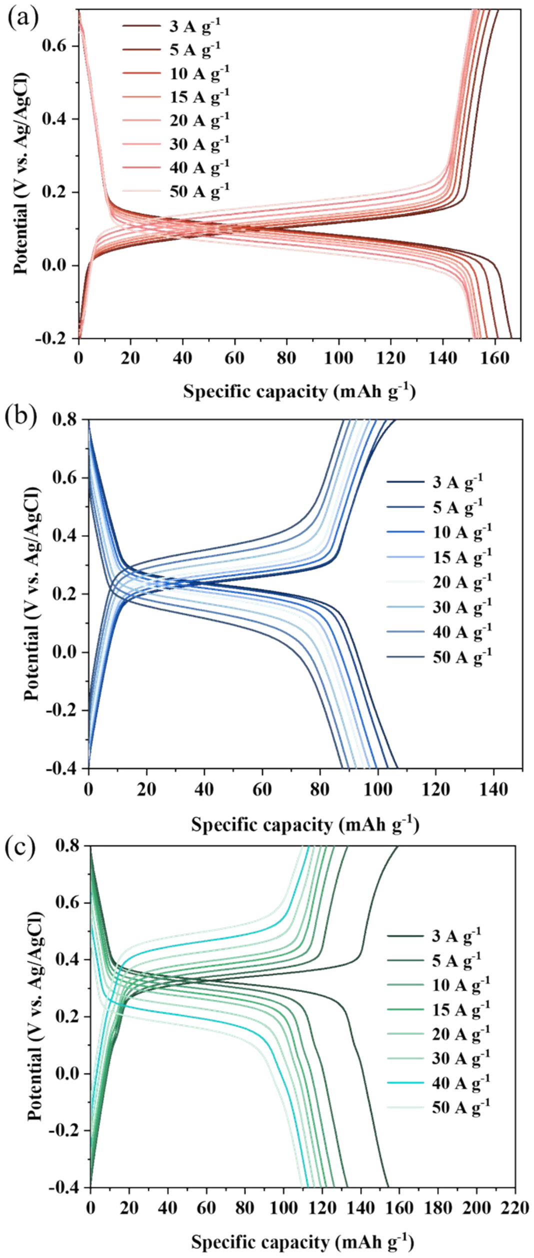

Fig. S12 The GCD curves of (a) TMBQ, (b) DMBQ, and (c) MBQ.

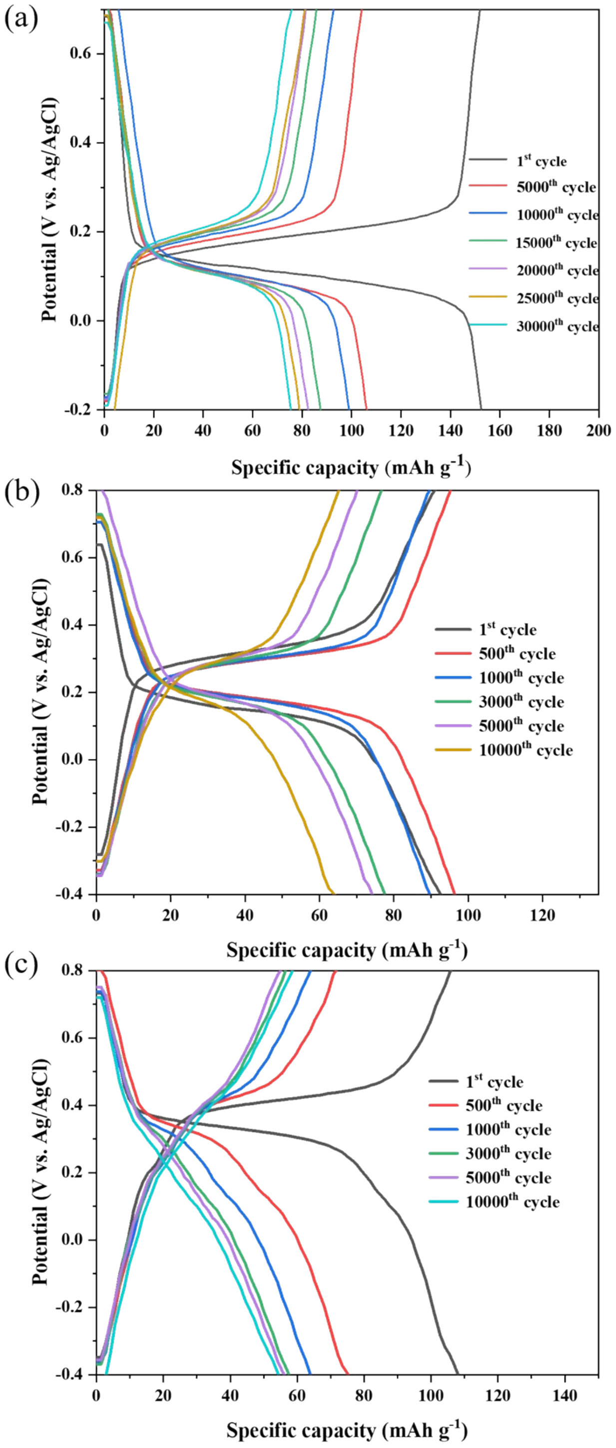

Fig. S13 The GCD curves of (a) TMBQ, (b) DMBQ, and (c) MBQ at selected cycles.

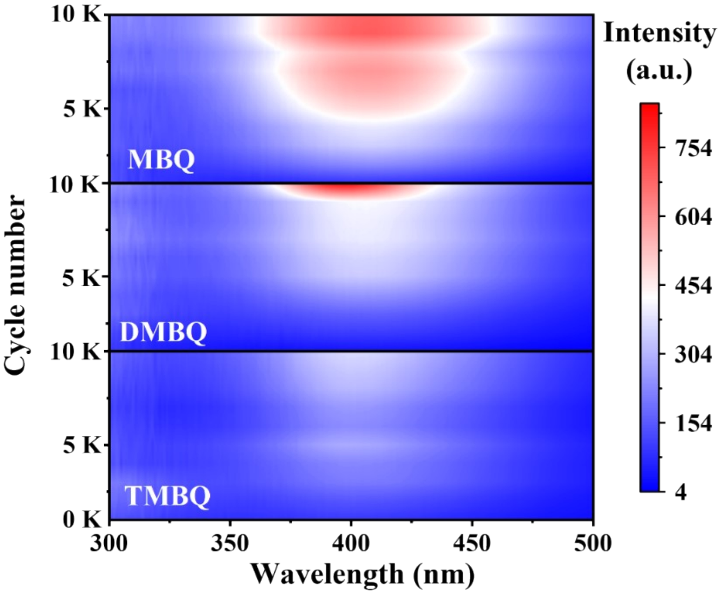

Fig. S14 The ex-situ UV-vis spectra of cycled electrolyte during the 10000 cycles of MBQ, DMBQ, and TMBQ.

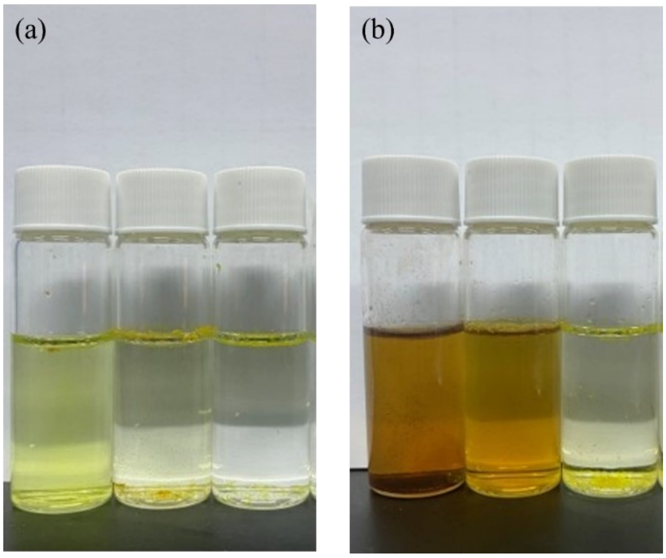

Fig. S15 Photograph of different materials in different electrolytes. From left to right, MBQ, DMBQ, and TMBQ in 0.5 M H_2SO_4. (a) At initial states. (b) After 7 days of soaking.

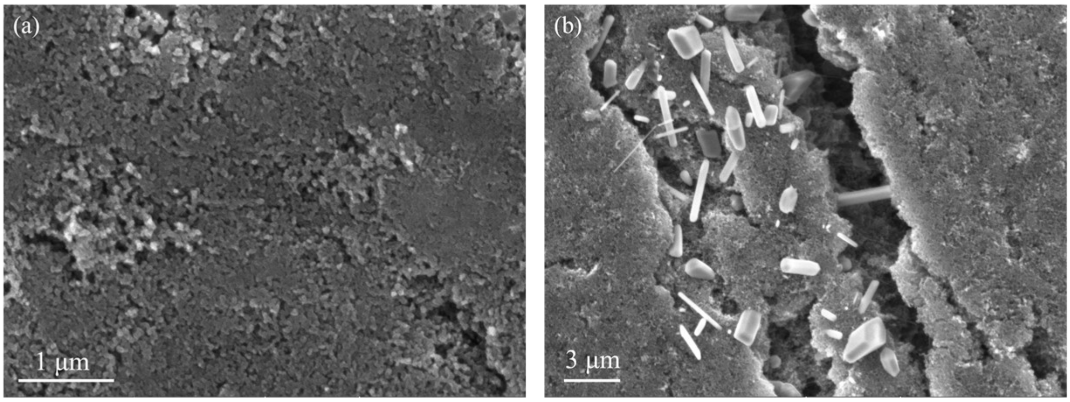

Fig. S16 SEM of MBQ. (a) At initial states. (b) After 10000 cycles in 0.5 M H_2SO_4.

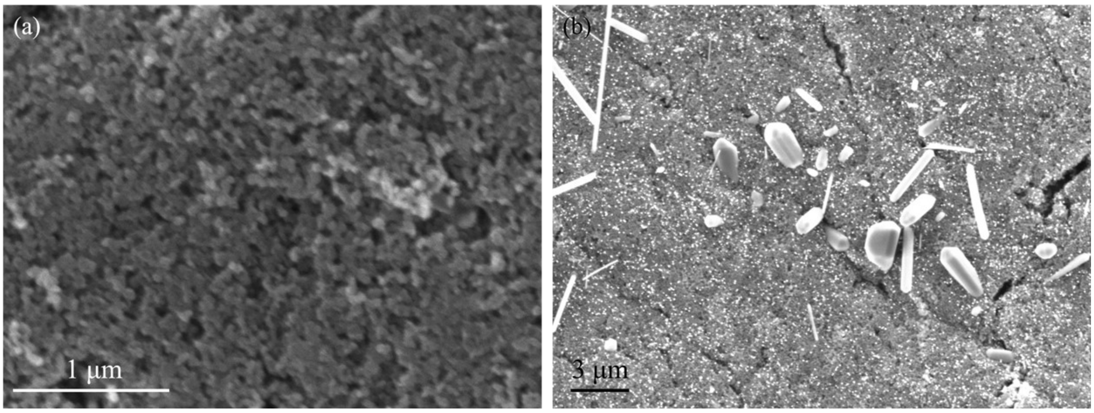

Fig. S17 SEM of DMBQ. (a) At initial states. (b) After 10000 cycles in 0.5 M H_2SO_4.

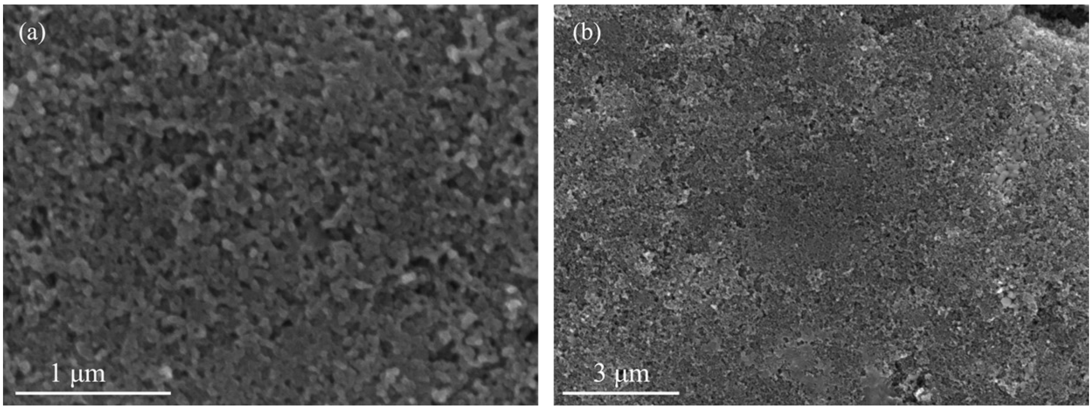

Fig. S18 SEM of TMBQ. (a) At initial states. (b) After 10000 cycles in 0.5 M H_2SO_4.

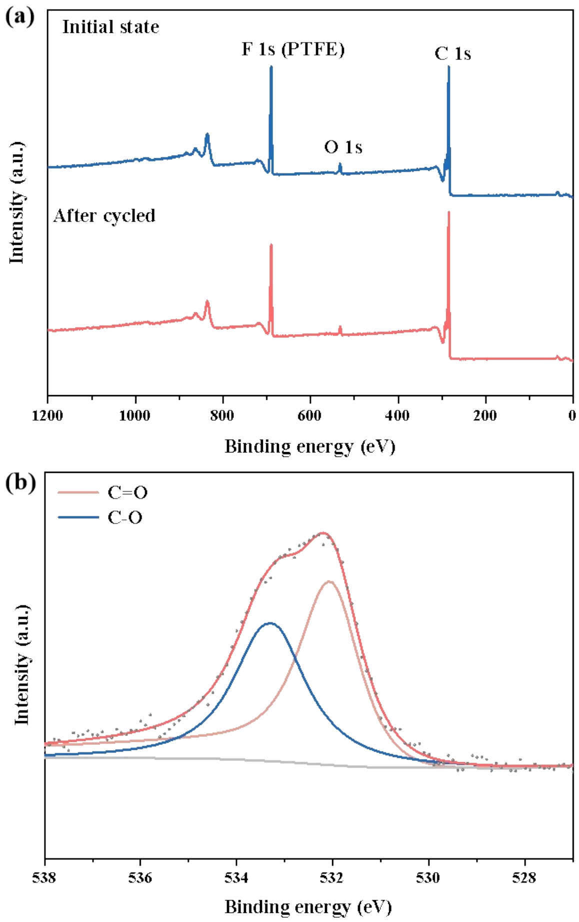

Fig. S19. (a) XPS survey spectra and (b) O 1s spectra of TMBQ before and after 30,000 cycles.

As shown in the full survey spectra (Fig. S19a), no significant attenuation in the C and O signals is observed, indicating that the elemental composition remains stable after prolonged cycling. Further comparison of the high-resolution O 1s spectra (Fig. S19b) shows that characteristic peaks corresponding to C=O and C–O functional groups are present after cycling, indicating that the redox-active quinone structure of TMBQ is largely retained.

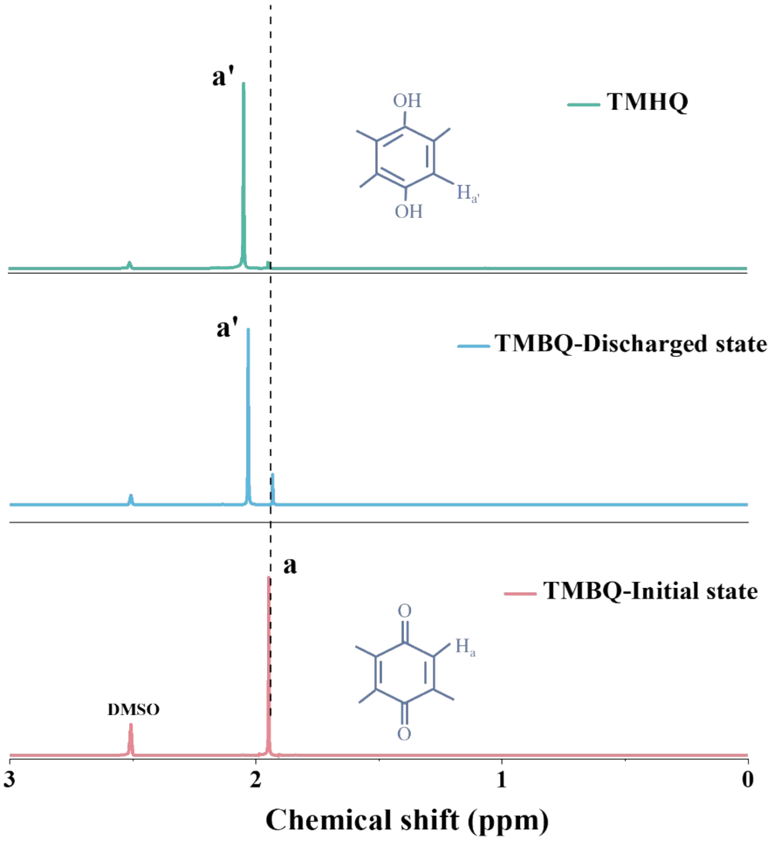

Fig. S20 ^{1}H NMR spectra of TMBQ at the initial state, discharged state, and for standard tetramethylhydroquinone (TMHQ).

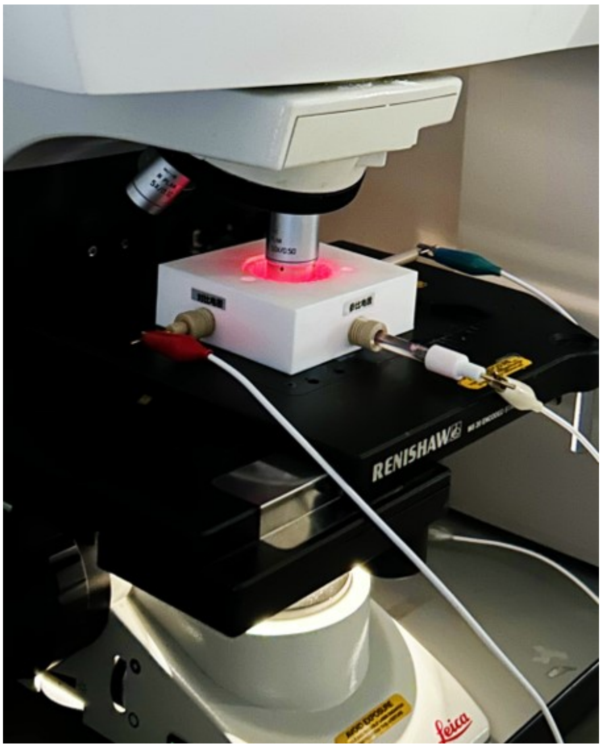

Fig. S21 The optical image of in-situ Raman device.

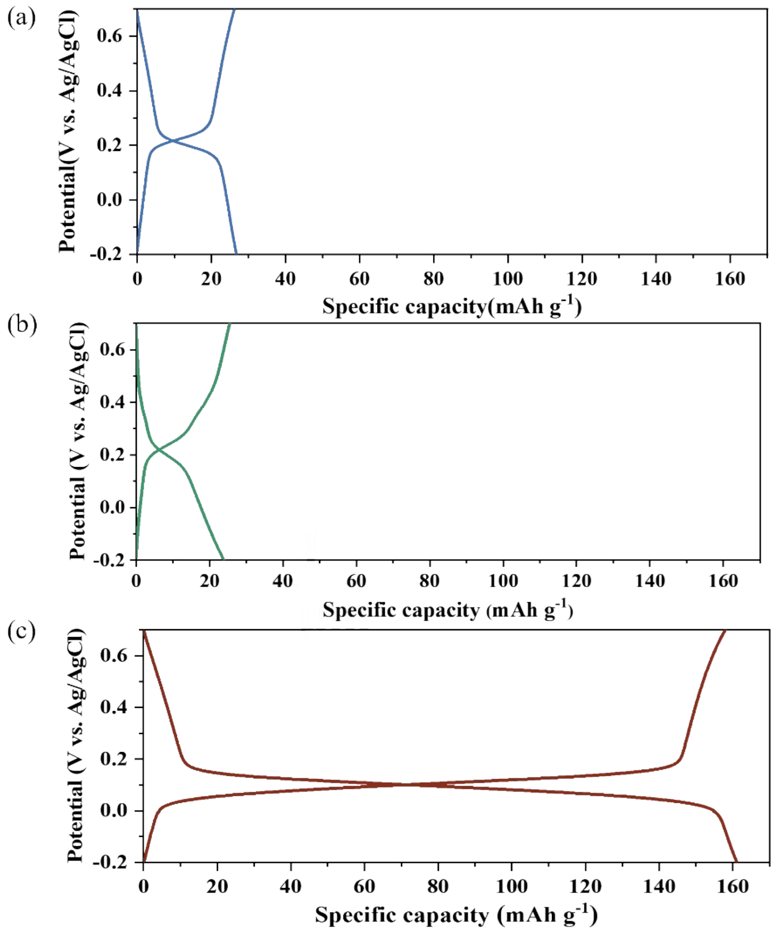

Fig. S22 GCD curves of (a) TMB, (b) Ketjen black, and (c) TMBQ at a current density of 5 A g^{-1} in 0.5 M H_2SO_4.

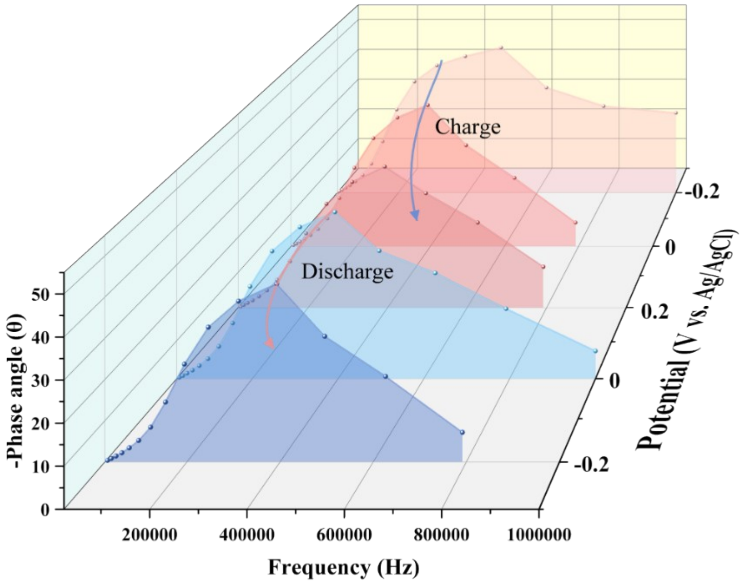

Fig. S23 Operando EIS analysis. Bode plots of TMBQ during the charge and discharge process.

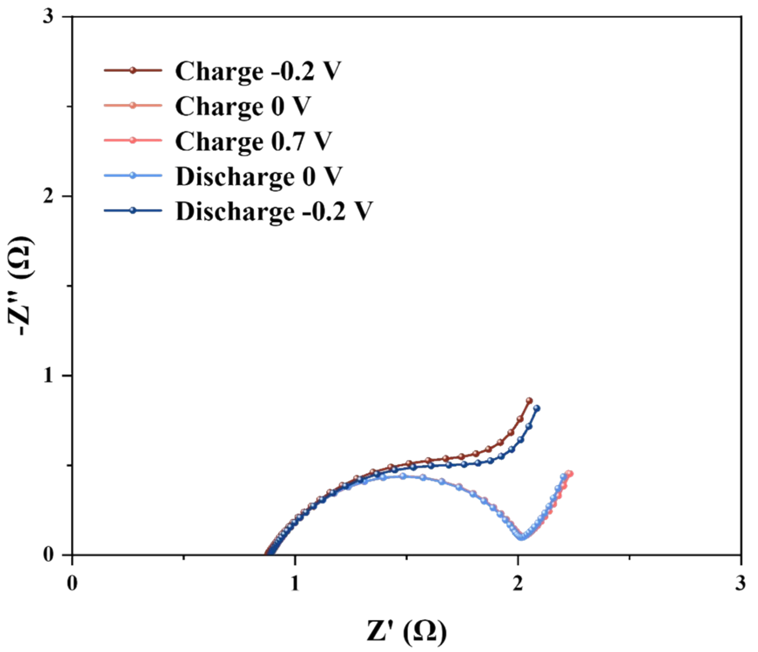

Fig. S24 Operando EIS analysis. Nyquist plots of TMBQ during the charge and discharge process.

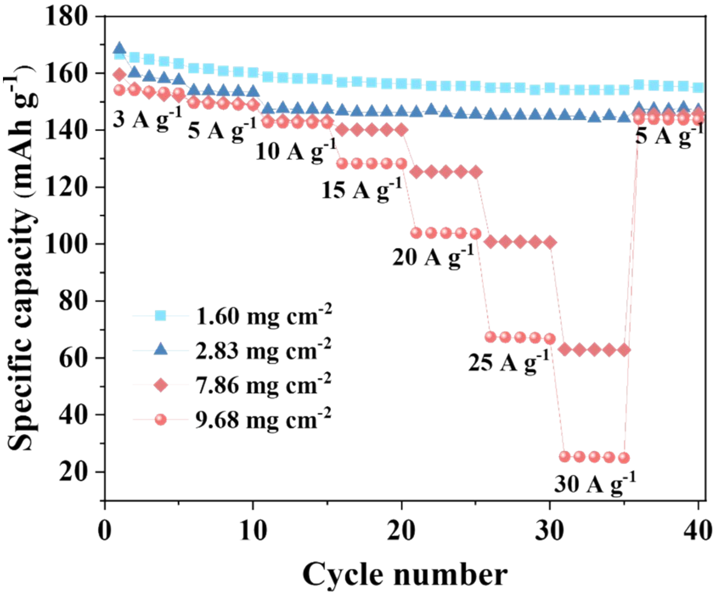

Fig. S25 The rate performance of TMBQ at different loading from 1.60 to 9.68 mg cm^{-2}.

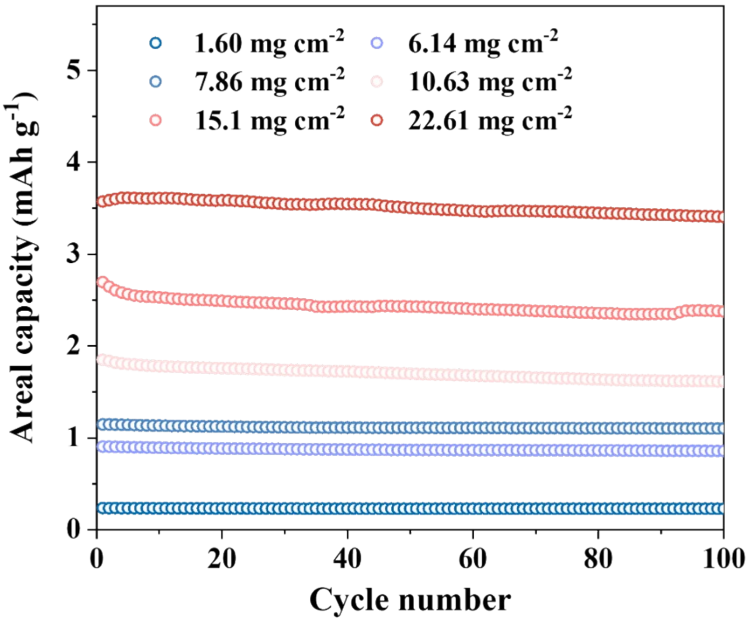

Fig. S26 The areal capacity over different loading at 50 mA cm^{-2} during 100 cycles.

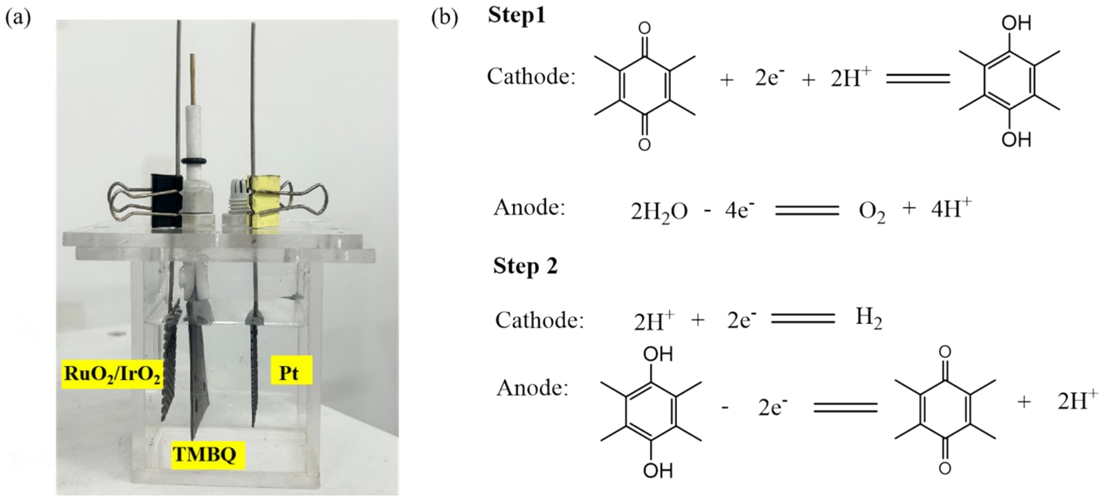

Fig. S27 The decoupled water electrolysis of (a) the optical image and (b) corresponding reaction equations.

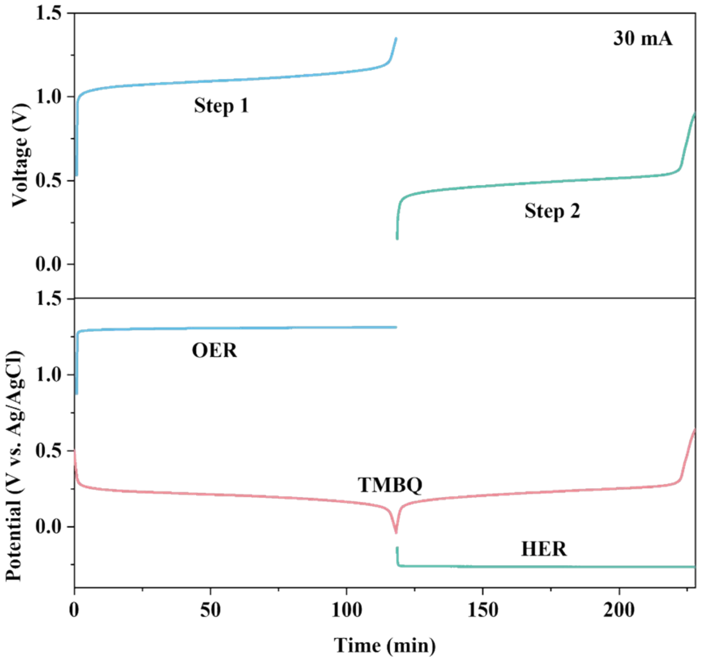

Fig. S28 Chronopotentiometry curves of TMBQ electrode tested at an applied current of 30 mA.

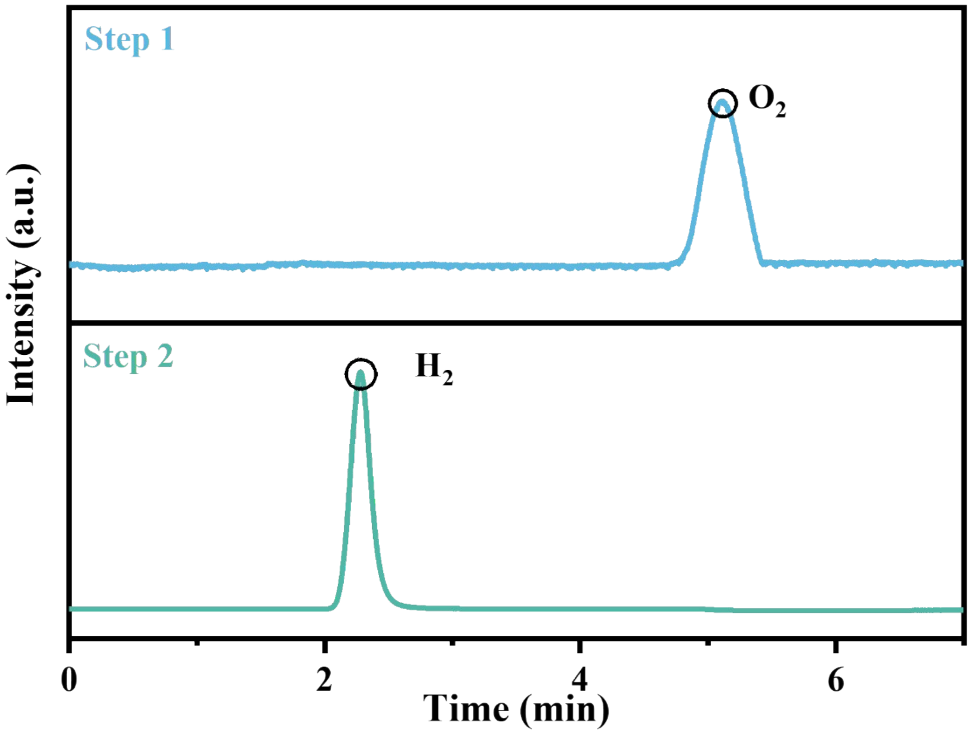

Fig. S29 Gas chromatography for O_2 and H_2 production.

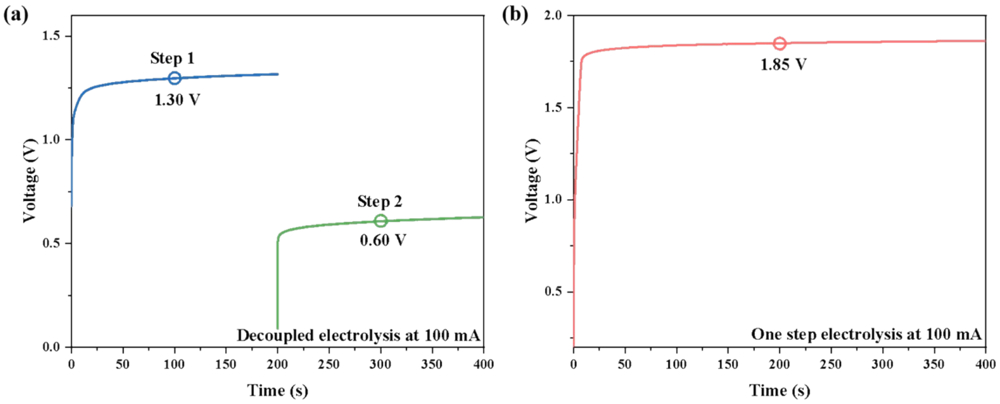

Fig. S30 Voltage comparison at 100 mA between (a) decoupled electrolysis and (b) one-step direct electrolysis without membrane.

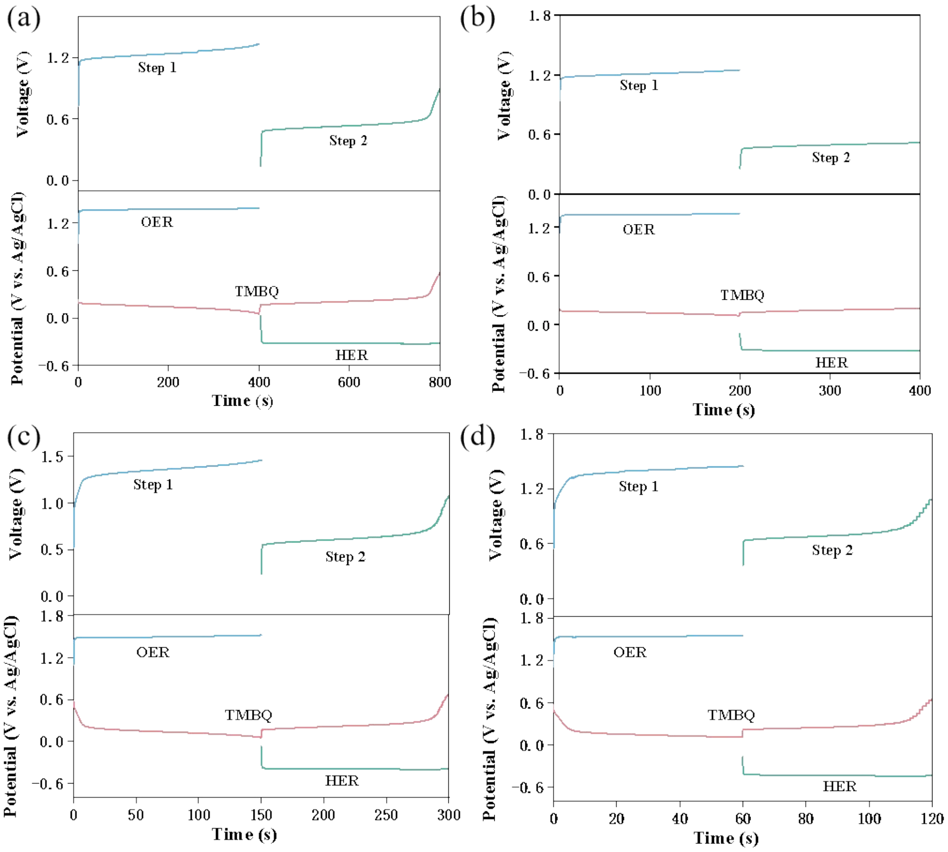

Fig. S31 Chronopotentiometry curve of the decoupled cell at a current of (a) 400 mA, (b) 300 mA, (c) 200 mA, and (d) 100 mA in 0.5 M H_2SO_4. The mass of redox mediator used was 150 mg.

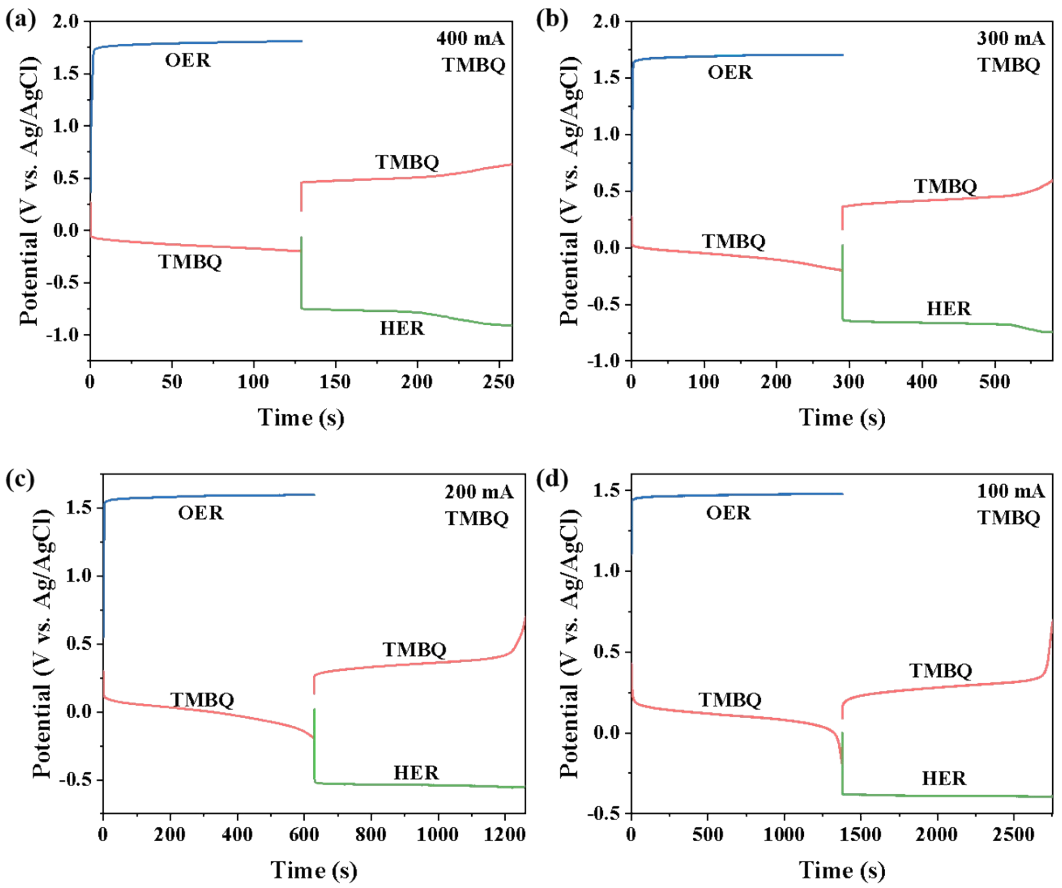

Fig. S32 Chronopotentiometry curve of the decoupled cell at a current of (a) 400 mA, (b) 300 mA, (c) 200 mA, and (d) 100 mA in 0.5 M H_2SO_4. The mass of redox mediator used was 400 mg.

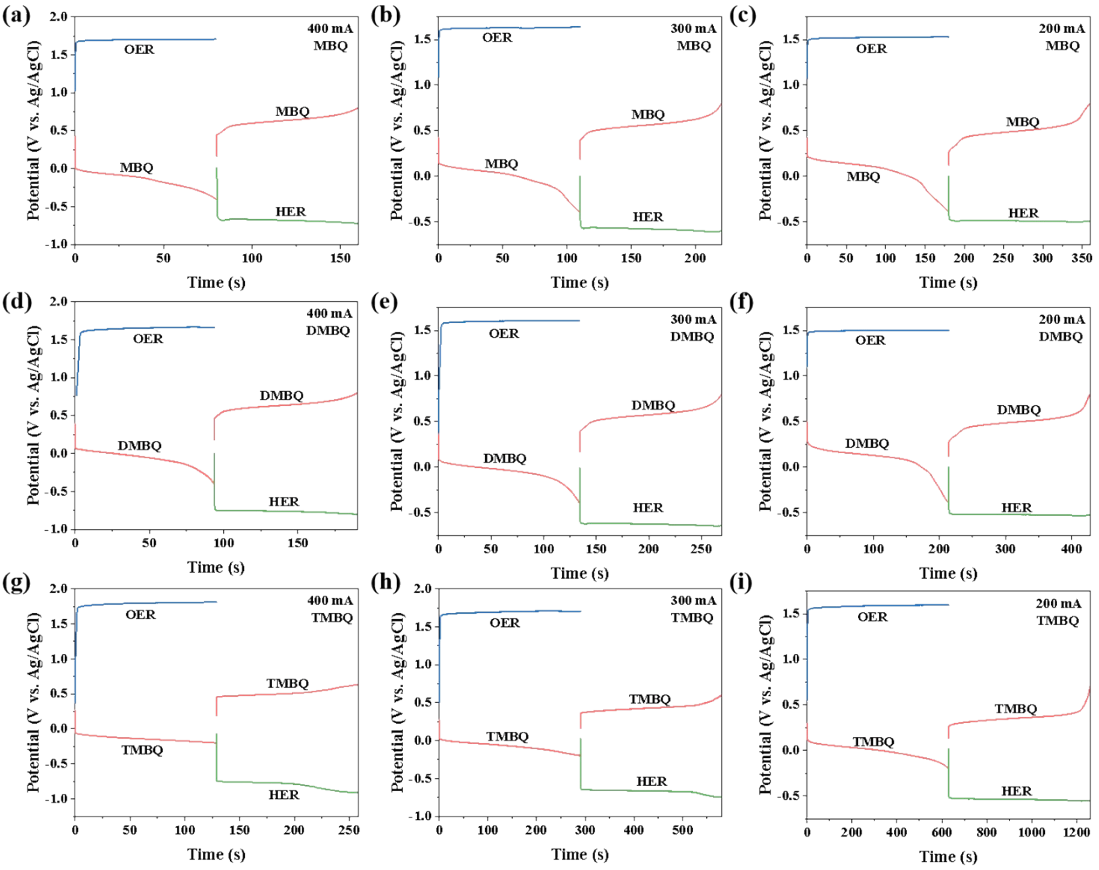

Fig. S33 Chronopotentiometry curves of the decoupled cell at different currents: (a–c) MBQ at the current of 400, 300, and 200 mA, respectively; (d–f) DMBQ at the current of 400, 300, and 200 mA, respectively; (g–i) TMBQ at the current of 400, 300, and 200 mA, respectively.

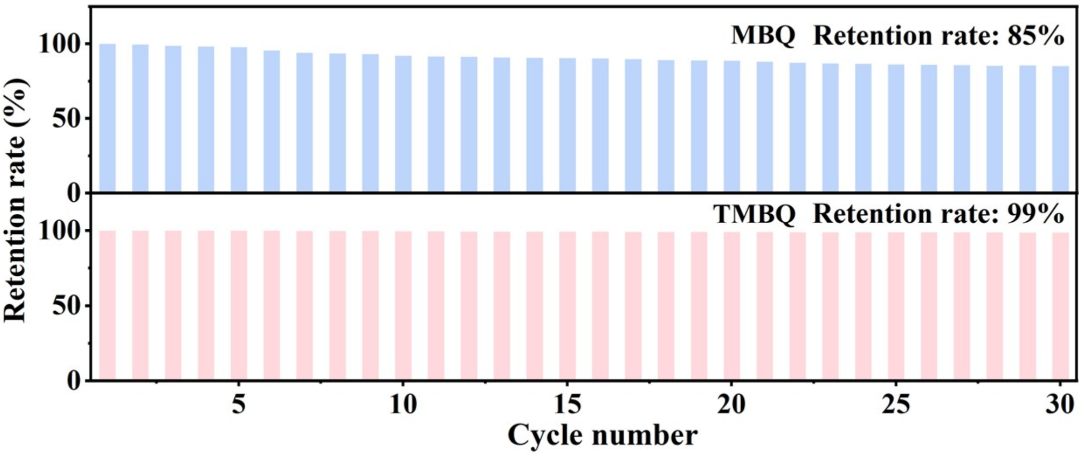

Fig. S34 The comparison of decoupled time stability between MBQ and TMBQ under thirty consecutive OER/HER cycles.

Table S1 Properties of the solid-state redox mediators for decoupled hydrogen production.

Solid-state redox mediator	Redox potential (V vs. RHE)	Reversible specific capacity (mAh g^{-1})	Stability (Cycles)	Ref.
CuFe-TBA	+0.71	80 (mAh g^{-1})	300	Adv. Energy Mater. 2023, 13, 2203455
PTO	+0.51	156 (0.2 A g^{-1})	300	Angew. Chem. Int. Ed., 2019, 58, 4622
MoO_3	+0.34	220 (5 A g^{-1})	1000	Adv. Funct. Mater. 2023, 33, 2214466
HATN	+0.52	260 (5 A g^{-1})	3000	Angew. Chem. Int. Ed. 2023, 135, e202303563
HVHCF	+0.80	126 (10 A g^{-1})	6000	Nat. Commun. 2024, 15, 1339
MBQ	+0.54	130 (5 A g^{-1})	10000	This work
DMBQ	+0.48	104 (5 A g^{-1})	10000	This work
TMBQ	+0.40	192 (5 A g^{-1})	30000	This work